

## Growth and characteristics of TaN/TiN superlattice structures

H. Wang<sup>a)</sup> and X. Zhang

*Materials Science and Technology Division, Los Alamos National Laboratory, Los Alamos, New Mexico 87545*

A. Gupta, Ashutosh Tiwari, and J. Narayan

*Department of Materials Science and Engineering, North Carolina State University, Raleigh, North Carolina 27695-7916*

(Received 23 January 2003; accepted 13 August 2003)

Epitaxial B1 NaCl-structured TaN(3 nm)/TiN(2 nm) superlattice structures were grown on Si(100) substrates with a TiN buffer layer, using pulsed-laser deposition. A special target assembly was used to manipulate the thickness of each layer. X-ray diffraction, transmission electron microscopy, and scanning transmission electron microscopy (*Z* contrast) studies confirmed the single-crystalline nature of the superlattice with a uniform layer structure. Nanoindentation results suggest the high hardness of these superlattice structures. Four-point-probe resistivity measurements show low resistivity of the heterostructures and a Cu diffusion characteristic study proved this superlattice system can be a promising diffusion barrier and can withstand 700 °C annealing for 30 min. © 2003 American Institute of Physics. [DOI: 10.1063/1.1616656]

TaN has become a very promising diffusion barrier material for Cu interconnects. Its high thermal stability, relatively dense interstitial structure, and low diffusion fulfill the requirements for next-generation ultra-large-scale integrated devices.<sup>1–3</sup> Recently, single crystal cubic TaN (B1–NaCl structure) has been integrated with Si via a thin layer of TiN and this configuration has emerged as a better Cu diffusion barrier material than other polycrystalline TaN barriers, mainly because it lacks grain boundaries which act as faster diffusion paths.<sup>4,5</sup> Besides, extensive research has shown that after high temperature annealing and subsequent breakdown, most of the Cu diffuses along the grain boundaries of barrier materials and segregates along the interface between Si and the diffusion barriers, finally extending into the underlying Si.<sup>1,6,7</sup> These special Cu diffusion profiles have been reasoned as: (1) Cu diffused into Si results in defect formation and Cu<sub>3</sub>Si precipitates in the Si substrate; and (2) possible chemical reactions between the barrier layer and Si substrate cause the interface failure.<sup>7</sup> In this letter, in order to avoid the Cu segregation along the Si/barrier interface and further diffusion into Si, we propose the additional interfaces built in the diffusion barrier could act as multiple segregation points and inhibit the Cu from further diffusing inside the barrier layer. Based on this idea, the epitaxial superlattice structure of TaN(3 nm)/TiN(2 nm) was synthesized on the Si(100) substrate by pulsed-laser deposition (PLD). The reason that we chose TiN as the other component is that it has a good diffusion barrier property, low electrical resistivity, good lattice match with cubic TaN, and well-established process technology in integrated circuit fabrication.

The depositions of the TiN buffer layer and TaN/TiN superlattice were performed in a multitarget chamber with a KrF excimer laser ( $\lambda = 248$  nm, 10 Hz). The laser beam was focused to obtain an energy density of approximately  $10 \text{ J cm}^{-2}$  at a 45° angle of incidence. The targets were hot-pressed stoichiometric TiN and TaN ob-

tained from CERAC, Inc. The target for superlattice deposition was specially arranged, as shown in Fig. 1. The ratio of the area of two targets, target rotation speed, and laser ablation frequency can be varied for engineering the thickness of each layer. A TiN buffer layer (about 10 nm) and TaN/TiN superlattice (200–500 nm) were deposited at a typical growth rate of 0.2 nm/s with a base pressure of about  $1 \times 10^{-8}$  Torr and substrate temperature  $650 \pm 10$  °C. The crystal structure of these films was determined by x-ray diffraction (XRD) using a Rigaku x-ray diffractometer with Cu *K* $\alpha$  radiation and a Ni filter. Microstructural characterization of these films was performed by transmission electron microscopy (TEM) and scanning transmission electron microscopy (STEM) using a JEOL-2010F analytical electron microscope with point-to-point resolutions of 0.18 nm (TEM) and 0.12 nm (STEM).

The XRD pattern (intensity versus  $2\theta$ ) of the TaN/TiN superlattice structure on Si(100) using TiN as buffer layers is shown in Fig. 2. The two main peaks centered at 42.27° and 93.05° are indexed as TaN/TiN superlattices (200) and (400), respectively, suggesting that the superlattice structures have grown highly aligned on Si(100). In addition, two small satellite peaks originating from the superlattice structure are clearly observed in the log-scale plot. Due to the fact that the lattice parameter of TiN (0.424 nm) is very close to that of B1–NaCl structured TaN ( $a = 0.433$  nm) with a lattice mis-



FIG. 1. Schematic configuration of the target assembly for deposition of the TaN/TiN superlattice by pulsed-laser deposition. Arrows indicate target rotation and laser beam direction, respectively.

<sup>a)</sup>Electronic mail: wangh@lanl.gov

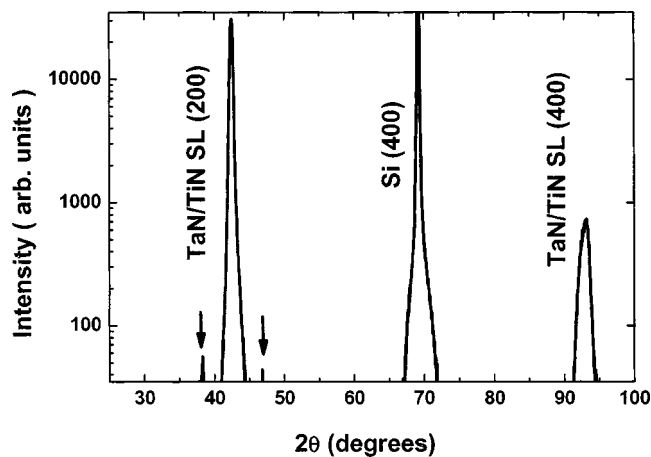


FIG. 2. XRD pattern (intensity vs  $2\theta$ ) showing (200) peaks and satellite peaks (marked by arrows) from the TaN/TiN superlattice on the Si(100) substrate.

match of only about 2%, the peaks for the TiN and TaN layers overlap to give a single diffraction peak, corresponding to a lattice parameter of  $a=0.426$  nm. The TiN buffer layer peaks are also merged with superlattice diffractions, so XRD gives mainly the diffractions from the TiN/TaN superlattice. It also proves that the B1-cubic metastable TaN phase has been stabilized by the cubic TiN buffer layer and by interposing TiN multilayers in the superlattice configuration.

Figure 3(a) shows the uniform superlattice structure from the  $\langle 110 \rangle$  cross-section sample of the TaN/TiN superlattice on Si with a TiN buffer layer. It is clear that the uniform superlattice structure forms throughout the whole sample above the 10 nm TiN buffer layer. The total thickness of the superlattice structure in this sample is about 250 nm, which corresponds to 50 bilayers of TaN (3 nm) and TiN (2 nm). In order to study the detailed interface structure between these superlattice layers, high resolution TEM was performed from the same area and shown in Fig. 3(b). The high resolution image clearly shows that the superlattice of TaN(3 nm)/TiN(2 nm) has grown epitaxially on the TiN buffer layer. The interfaces between TiN and TaN are sharp and clean without

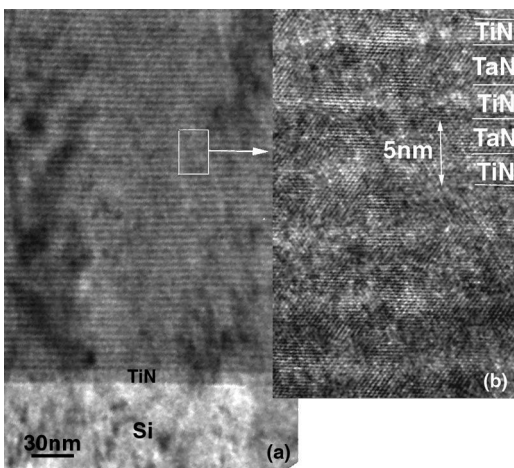


FIG. 3. (a) Low magnification and (b) high resolution TEM image of the  $\langle 110 \rangle$  cross-section sample of the TaN(3 nm)/TiN(2 nm) superlattice on Si(100) using a TiN buffer layer ( $\sim 10$  nm), showing a uniform layer structure has formed throughout the sample thickness.

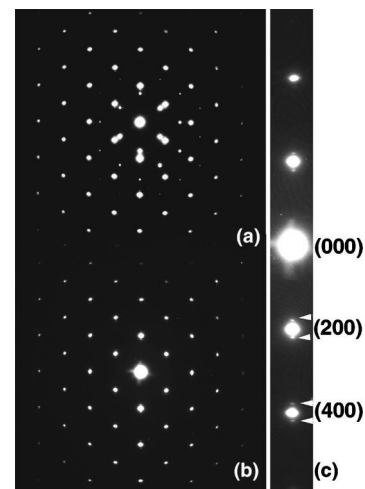


FIG. 4. SAD pattern of the  $\langle 110 \rangle$  cross-section sample of the TaN(3 nm)/TiN(2 nm) superlattice on Si(100): (a) diffraction from the superlattice and substrate; (b) diffraction from the superlattice only; and (c) magnified (200) diffraction set indicating the satellite feature for the superlattice structure.

any indication of interface reaction. The lattice mismatch between TiN and TaN is within 2%, which leads to the lattice matching epitaxy growth of these two layers. The  $\{111\}$  lattice planes of these two materials are well aligned. Some dislocations generated from the TiN buffer layer and further extended into TaN/TiN superlattice were observed in Fig. 3(a). These may be reduced by improving the TiN buffer layer quality. The interface structure and domain matching epitaxy of TiN on Si has been discussed in detail elsewhere.<sup>4,8</sup> Basically, the extra half plane generated in TiN accommodates the large lattice strain (24%) and forms four planes of TiN lattice matching with three planes of Si lattice giving a lattice mismatch about 4%.<sup>8</sup> The additional misfit is relaxed by the domain matching variation as discussed in detail.<sup>9</sup> That is one of the reasons why the TiN buffer layer was chosen for epitaxial growth of the TaN/TiN superlattice. Another reason is that the TaN phase directly deposited on Si(100) or Si(111) was found to be polycrystalline hexagonal  $\epsilon$ -TaN, which is the stable phase of TaN, and the same as the target. The formation of metastable B1 NaCl-structured TaN is facilitated by the lattice matching with TiN and the non-equilibrium characteristics of PLD (the average energy of laser ablated species  $\sim 100$ – $1000$  kT).

Selected area diffraction (SAD) patterns from the  $\langle 110 \rangle$  cross-section sample of the superlattice TaN/TiN on Si(100) are shown in Fig. 4. Diffractions from the superlattice plus substrate and only from the superlattice are shown in Figs. 4(a) and 4(b), respectively. The epitaxial relation for the superlattice and substrate is determined to be the TaN/TiN superlattice  $\langle 110 \rangle \parallel$  TiN  $\langle 110 \rangle \parallel$  Si  $\langle 110 \rangle$  with a cubic-on-cubic epitaxial relationship. Figure 4(b) shows only the diffraction from the TaN/TiN superlattice indicating the high quality of the superlattice with calculated lattice parameter of 0.4260 nm, which is very close to that of TiN. For 2% lattice mismatch between TaN and TiN, the TaN film can grow coherently on TiN within a 3-nm-thick layer. Thus, a highly aligned superlattice is formed having a structure very similar to TiN. The set of the (200) diffraction spot superlattice structure is magnified and shown in Fig. 4(c), where the satellite diffractions around transmitted beam (000) and dif-

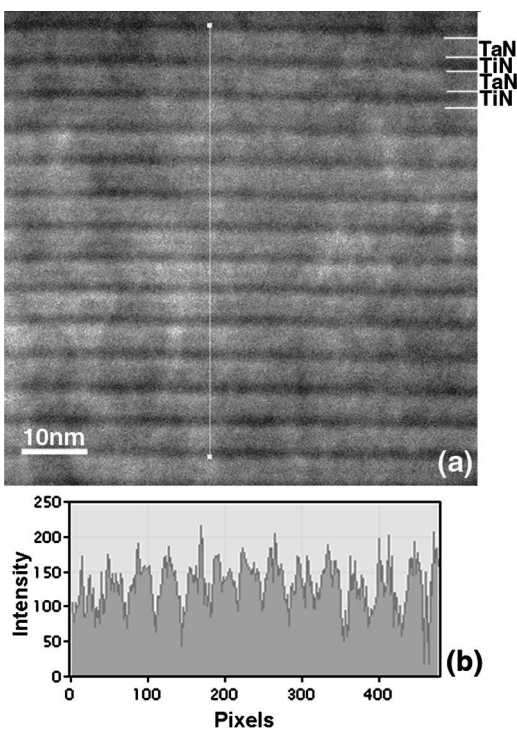


FIG. 5. (a) STEM (Z-contrast) image from the TaN/TiN superlattice structure indicating the layer structure and elemental uniformity; (b) Z-contrast intensity plot showing that the intensity varies periodically from different TaN and TiN layers.

fracted beam (200), (400) are clearly visible, indicating the superlattice structure formed parallel to the (200) plane.

The elemental distribution is studied by STEM (Z contrast) on a  $\langle 110 \rangle$  cross-section sample of the superlattice TaN/TiN on Si(100). A STEM image from the superlattice clearly showed a uniform layer structure and sharp interfaces of TaN/TiN without any indication of interfacial reactions, as shown in Fig. 5(a). The TaN layers have a brighter contrast compared to TiN, because the contrast of the STEM image is proportional to  $Z^2$  and the atomic number of Ta is 73, much larger than that of Ti (22). The corresponding intensity profile of the superlattice structure is plotted in Fig. 5(b), which clearly shows that the Z contrast varies periodically as the beam scanned through different TaN and TiN layers.

The hardness of the TaN/TiN superlattice structures with thickness over 500 nm, was measured by nanoindentation techniques. The measured hardness of these superlattice structures is about 26 GPa, which is much higher than the rule-of-mixtures value (16.6 GPa) of TaN and TiN. The resistivity of these superlattice structures over the temperature range 12–300 K was measured by four-point probe. Their room temperature resistivity is determined to be  $\sim 130 \mu\Omega \text{ cm}$  with a rather small temperature coefficient of resistivity of  $0.002 \text{ K}^{-1}$ .

In order to determine the Cu diffusion barrier properties of these epitaxial cubic TaN/TiN superlattices, a layer of Cu film was deposited on a superlattice at room temperature and annealed at 700 °C in vacuum for 30 min. In Fig. 6, the high resolution TEM image of the  $\langle 110 \rangle$  cross-section sample of the Cu/TaN–TiN superlattice/TiN/Si(100) after annealing is clearly observed, in which the interface between the Cu and TaN/TiN superlattice remains very sharp without any indication of Cu diffusion or interfacial reaction. Compared with

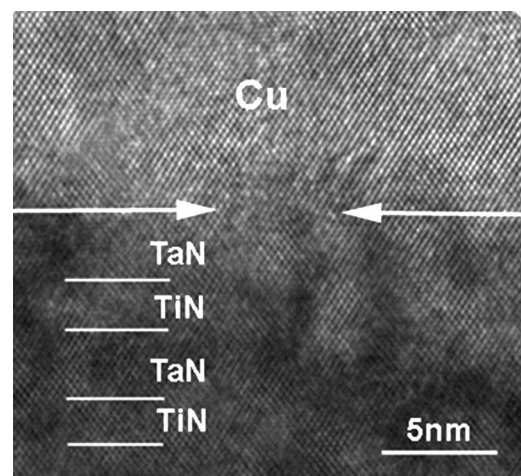


FIG. 6. High magnification TEM image of the  $\langle 110 \rangle$  cross-section sample of the Cu/TaN–TiN superlattice/TiN/Si(100) after 700 °C annealing for 30 min.

other reports, the diffusion barrier property of this new structure is better than TaN itself<sup>10</sup> and much better than TiN.<sup>11</sup> The high barrier efficiency of this superlattice structure is explained as follows: first, TaN/TiN superlattice structures have a layer-by-layer structure and each of the layers can act as an efficient diffusion barrier because TaN and TiN are high temperature materials with very high melting points (TaN, 3087 °C and TiN, 2950 °C) and high bulk diffusion activation energy; second, the interfaces between TaN and TiN in the superlattice may provide preferential Cu segregation points as the interface normally has a higher defect density and strain stress than the bulk region. The detailed interface diffusion study is continuing in our laboratory by higher temperature annealing.

In conclusion, epitaxial TaN/TiN superlattices with uniform layer structure have been grown on Si(100) substrates with TiN as a buffer layer using PLD. TEM and STEM (Z-contrast) studies have proved the single crystal nature and uniformity of the superlattice structures. Cubic B1–NaCl-structured TaN is stabilized by thin layers of TiN in the superlattice and TiN buffer layer. High hardness, low resistivity, and promising Cu diffusion characteristics all suggest that these superlattice structures could have future applications in Cu interconnects and superhard coatings.

<sup>1</sup>M. Stavrev, C. Wenzel, A. Moller, and K. Drescher, *Appl. Surf. Sci.* **91**, 257 (1995).

<sup>2</sup>P. Murarka, *Mater. Sci. Eng., R.* **19**, 87 (1997).

<sup>3</sup>G. S. Chen, S. C. Huang, S. T. Chen, T. J. Yang, P. Y. Lee, J. H. Jou, and T. C. Lin, *Appl. Phys. Lett.* **76**, 2895 (2000).

<sup>4</sup>H. Wang, A. Tiwari, A. Kvit, X. Zhang, and J. Narayan, *Appl. Phys. Lett.* **80**, 2323 (2002).

<sup>5</sup>H. Wang, A. Tiwari, X. Zhang, A. Kvit, and J. Narayan, *Appl. Phys. Lett.* **81**, 1453 (2002).

<sup>6</sup>M. H. Tsai, S. C. Sun, C. E. Tsai, S. H. Chuang, and H. T. Chiu, *J. Appl. Phys.* **79**, 6932 (1996).

<sup>7</sup>K. H. Min, K. C. Chun, and K. B. Kim, *J. Vac. Sci. Technol. B* **14**, 3263 (1996).

<sup>8</sup>J. Narayan, P. Tiwari, X. Chen, J. Singh, R. Chowdhury, and T. Zheleva, *Appl. Phys. Lett.* **61**, 1290 (1992); J. Narayan, U.S. Patent No. 5, 406,123 (1995).

<sup>9</sup>J. Narayan and B. C. Larsen, **93**, 278 (2003).

<sup>10</sup>T. Oku, E. Kawakami, M. Uekubo, K. Takahiro, S. Yamaguchi, and M. Murakami, *Appl. Surf. Sci.* **99**, 265 (1996).

<sup>11</sup>K. Y. Lim, Y. S. Lee, Y. D. Chung, I. W. Lyo, C. N. Whang, J. Y. Won, and H. J. Kang, *Appl. Phys. A: Mater. Sci. Process.* **70**, 431 (2000).